

The catalytic potential of biosynthesized silver nanoparticles from *Malva Sylvestris* and *Beetroot* extracts for methylene blue reduction

Sima Mehdizadeh¹, Nahid Ghasemi^{1,2}

¹Department of chemistry, Ashtian Branch, Islamic Azad University, Ashtian, Iran

²Department of Chemistry, Arak Branch, Islamic Azad University, Arak, Iran

ABSTRACT

ARTICLE INFO

Article History:

Received 2024-07-24

Accepted 2024-09-03

Published 2023-09-15

Keywords:

Biosynthesis,

Silver Nanoparticles,

Malva Sylvestris,

Beetroot,

Catalytic degradation.

Silver nanoparticles (AgNPs) were effectively synthesized via a biosynthesis method using aqueous extracts of *Malva Sylvestris* (MS) and *Beetroot* (BR). The phenolic and flavonoid compounds in these extracts served as potent reducing and stabilizing agents. A comprehensive investigation was conducted to examine the effect of various synthesis parameters, including pH, extract volume, salt concentration, temperature, and time, on the formation of nanoparticles. The synthesized AgNPs were characterized using ultraviolet-visible (UV-Vis) spectrophotometry, X-ray diffraction (XRD), scanning electron microscopy (SEM), transmission electron microscopy (TEM), and Fourier-transform infrared spectroscopy (FT-IR). Both types of AgNPs exhibited a face-centered cubic crystal structure, with maximum absorbance peaks at 439 nm for AgNPs.BR and 434 nm for AgNPs.MS. Catalytic activity in reducing methylene blue was verified through surface plasmon resonance (SPR) spectroscopy. Kinetic data were analyzed using pseudo-first-order, pseudo-second-order, intraparticle diffusion, and Elovich models. The enhanced reduction of methylene blue (MB) in the presence of 0.008 g AgNPs.BR and 0.005 g AgNPs.MS, with rate constants of 0.024 min⁻¹ and 0.097 min⁻¹ respectively, demonstrated the significant catalytic potential of these nanoparticles.

How to cite this article

Mehdizadeh S., Ghasemi N., The catalytic potential of biosynthesized silver nanoparticles from *Malva Sylvestris* and *Beetroot* extracts for methylene blue reduction. *J. Nanoanalysis.*, 2023; 10(3): 542-559.

INTRODUCTION

The burgeoning textile industry has generated

a significant environmental concern due to the release of synthetic dyes, including MB, into water bodies.

*Corresponding Author Email: n-ghasemi@iau-arak.ac.ir



This work is licensed under the Creative Commons Attribution 4.0 International License.

To view a copy of this license, visit <http://creativecommons.org/licenses/by/4.0/>.

MB, a cationic dye with an intense blue color, is toxic and persistent in the environment, posing a threat to aquatic life and human health [1]. Conventional wastewater treatment methods, such as physical and chemical processes, often fall short in effectively removing MB due to its high stability and resistance to biodegradation [2]. In recent years, nanotechnology has emerged as a promising approach for wastewater treatment, offering a viable alternative to conventional methods. Among the diverse nanomaterials, silver nanoparticles AgNPs have garnered significant attention due to their unique physicochemical properties, including high surface area, antimicrobial activity, and catalytic potential [3]. The synthesis of AgNPs using plant extracts, known as plant-mediated synthesis, offers a sustainable and eco-friendly approach to nanomaterial production [4].

Scientists value the biosynthesis of nanoparticles, which utilize plant extracts as both reducing and capping agents. This approach has transformed traditional nanomaterial synthesis, which relied primarily on chemical processes. The simplicity and biocompatibility of the biosynthesis technique have appealed to researchers for years, making it a sustainable and cost-effective option for nanoparticle synthesis.

Silver nanoparticles are among the noble metals that have been successfully utilized to create nanoparticles using various methods, including chemical reduction, microemulsions, hybrid methods, photochemical reduction, sonoelectrochemical, and microwave-based systems. The production of silver nanoparticles in a green manner, with the help of plants, has gained significant attention in recent years due to the environmental concerns associated with traditional synthetic methods that rely on hazardous chemicals or are expensive. Green synthetic techniques utilize naturally occurring reducing and capping agents, such as plant extracts, sugars, biodegradable polymers, and microbes, to produce nanoparticles.

Plant extracts are becoming a popular choice as reducing and capping agents due to their low toxicity, cost-effectiveness, and lack of requirement for long-term collection of microbial cultures. The use of plant-derived nanomaterials is a promising area of research, due to their potential to create nanomaterials with unique properties and applications while also being sustainable and environmentally friendly.

Plant extracts contain a rich array of bioactive compounds, such as polyphenols, flavonoids, and carbohydrates, which can act as reducing and stabilizing agents during the synthesis of AgNPs [5]. These biomolecules facilitate the formation of AgNPs with controlled size, morphology, and dispersity [6]. The plant-mediated synthesis of AgNPs has gained significant momentum in recent years due to its simplicity, cost-effectiveness, and environmental friendliness. Researchers have explored a wide range of plant extracts for the synthesis of AgNPs with diverse properties and applications.

Numerous studies have demonstrated the successful synthesis of AgNPs using various plant parts such as leaves, roots, seeds, stems, and fruits. For example, plants like *Rosmarinus officinalis*[7], *Illicium verum*[8], *Gloriosa superba*[9], *Cassia tora*[10], *Phlomis*[11], *pennyroyal*[12], *Ferula persica*[13], *Lantana camara*[14], *Eucalyptus*[15], *Malva parviflora*[16], *Butea monosperma*[17], and *Rosa indica*[18] have been used in AgNPs synthesis.

Several studies have demonstrated the effectiveness of biosynthesized silver nanoparticles in catalytic dye reduction and detection applications. In 2023, Moond et al. [19] synthesized AgNPs using an aqueous extract of *fenugreek* (*Trigonella foenum-graecum* L.) leaves and demonstrated their efficacy in removing MB, methyl orange (MO), and rhodamine B (RhB) dyes from wastewater. The AgNPs exhibited excellent catalytic activity, leading to a significant reduction in MB concentration within a short time frame. Samari et al. utilized *mango* leaf extract to

synthesize AgNPs, which effectively reduced MB and (RhB) dyes in 12 and 8 minutes, respectively [20]. In 2023, Sharmin et al. [21] reported the synthesis of AgNPs using *Leea macrophylla* (LM) leaf extract, which is rich in phytochemicals. These biogenic AgNPs exhibited promising antibacterial and catalytic activities, highlighting the potential of LM extract for green nanomaterial production with diverse applications. Sooraj et al. reported the green synthesis of AgNPs using *Sida retusa* leaf extract, with the nanoparticles catalyzing NaBH₄ reduction of MB and MO, achieving complete reduction within 10 and 9 minutes, respectively [22].

These studies highlight the potential of plant-mediated AgNPs synthesis for developing sustainable and eco-friendly solutions for dye removal.

Nowadays, organic dyes are the primary cause of water pollution, making them the main contributors to severe contamination. Many industries, including those in textiles, paper, food, pharmaceuticals, cosmetics, leather, and printing, use organic dyes extensively as colorants, such as those present in the textile, paper, culinary, pharmaceutical, cosmetic, leather, and printing sectors. Due to their severe health risks, it is crucial to remove organic dyes specifically from drinking water.

On the basis of the above-mentioned information, MS and Beetroot plants were chosen as reduction agents for synthesis of silver nanoparticles. Specifically, MS, a common herb with a rich history of medicinal use, contains bioactive compounds such as polysaccharides, polyphenols, vitamins, mucilage, flavonoids, and unsaturated fatty acids, which have significant antioxidant, anti-inflammatory, and therapeutic effects. BR, a culinary vegetable, another valuable plant, is rich in vitamins and antioxidants like polyphenols and betalains, which have notable antioxidant, anti-inflammatory, hepatoprotective, and antitumor properties [23, 24]. The presence of these bioactive molecules in MS and BR extracts makes

them promising candidates for reducing and stabilizing AgNPs biosynthesis.

This study investigates the optimal synthesis conditions and assesses the influence of various parameters, including pH, extract volume, salt concentration, temperature, and time, on nanoparticle synthesis. The green-synthesized AgNPs were characterized using UV-Vis spectrophotometry, FT-IR, XRD, SEM, and TEM techniques. Furthermore, their catalytic activity in the reduction of MB in the presence of sodium borohydride (NaBH₄) was examined. Understanding the kinetics of dye removal is crucial for optimizing wastewater treatment processes and designing efficient adsorbent systems. Various kinetic models have been employed to describe the adsorption of dyes onto silver nanoparticles AgNPs in their catalytic activity.

In this study, we investigated the kinetics of MB removal using AgNPs synthesized from aqueous extracts of MS and BR. The pseudo-first-order, pseudo-second-order, intraparticle diffusion, and Elovich models were employed to analyze the adsorption mechanism.

EXPERIMENTAL

Reagents

Fresh samples of BR and MS were obtained from a local market in Arak, Iran. All chemicals, including silver nitrate (AgNO₃), NaBH₄, and MB, were purchased from Merck Company.

Preparation of BR and MS Extracts

The preparation of BR and MS extracts followed the method described in our previous work [25, 26]. Briefly, fresh BR and MS samples were thoroughly washed with tap water followed by deionized water to remove any impurities. The washed samples were then shade-dried at room temperature and finely ground using a mortar and pestle. Subsequently, 10 g of the BR or MS powder was mixed with 100 mL of deionized water and boiled for 5

minutes. The boiled mixtures were filtered, and the filtrates were centrifuged at 4000 rpm. The resulting extracts were stored in a refrigerator for further experiments.

Biosynthesis of silver nanoparticles

AgNPs were biosynthesized using fresh BR and MS extracts. A stock solution of 0.0045 M AgNO₃ was prepared by dissolving the appropriate amount of AgNO₃ in 100 mL of deionized water. The addition of the plant extracts to the AgNO₃ solution resulted in a color change to brown. This color change is attributed to the reduction of Ag⁺ ions to metallic Ag⁰ nanoparticles and the excitation of SPR within the nanoparticles, indicating their successful formation. Several key parameters, such as extract volume, salt solution concentration, pH, temperature, and reaction time, can influence the properties of the synthesized nanoparticles. We have previously investigated the effect of these parameters to establish the optimal conditions for the green synthesis of AgNPs using BR and MS extracts. The synthesized AgNPs from BR and MS extracts were named AgNPs.BR and AgNPs.MS, respectively. These nanoparticles were subsequently characterized using various techniques, including UV-visible spectroscopy, FT-IR, XRD, SEM, and TEM to determine their morphology, composition, and crystalline structure.

Characterization Techniques

The morphology, composition, and crystalline structure of the AgNPs were investigated using various instrumental techniques. UV-Vis spectroscopy was employed to analyze the samples in the wavelength range of 300–800 nm using an Agilent 8541 spectrophotometer. FT-IR spectroscopy was performed on the samples in the range of 400–4000 cm⁻¹ using a Perkin Elmer Spectrum spectrophotometer. XRD patterns were obtained using a Philips X'pert Pro X-ray diffractometer with Cu K α radiation ($\lambda = 1.54 \text{ \AA}$). Finally, the morphology of the AgNPs was visualized using SEM on a VEGAS-

TESCAN instrument and TEM on a Philips CM120 instrument.

Evaluation of Catalytic Activity for Methylene Blue Reduction

The catalytic activity of the biosynthesized silver nanoparticles (AgNPs.BR and AgNPs.MS) was assessed using the reduction of MB dye in the presence of NaBH₄ as a model reaction. This reaction system is widely employed for evaluating the catalytic potential of nanomaterials due to its simplicity and the well-defined characteristic peak of MB in the UV-visible spectrum.

To prepare the catalyst solutions, known quantities of AgNPs.BR (0.008 g) and AgNPs.MS (0.005 g) were individually dispersed in 25 mL of deionized water using ultrasonication for a specified time to achieve homogeneous dispersion. This step is crucial for maximizing the available surface area of the AgNPs, which is essential for optimal catalytic activity.

The reaction mixture for testing the catalytic activity of the synthesized AgNPs was prepared by adding a predetermined volume (100 μ L) of 0.01 M NaBH₄ solution to the dispersed AgNPs. The dispersion and NaBH₄ solution were then mixed thoroughly. Subsequently, a specific volume (3 mL) of MB solution at 10 μ M concentration was added to the reaction mixture to initiate the reduction reaction.

The reduction of MB dye was monitored by measuring its absorbance spectrum at different reaction times using a UV-visible spectrophotometer. MB exhibits a characteristic absorption peak at a specific wavelength (665 nm) in its oxidized form. Gradually decreasing the intensity of this peak indicates the conversion of MB to its colorless form as the reduction reaction progresses. The decrease in absorbance at the peak wavelength can be quantified and used to calculate the reaction rate and the catalytic efficiency of the AgNPs.

RESULTS AND DISCUSSIONS

Effect of influential Parameters on Silver Nanoparticle Synthesis

The influence of crucial parameters on AgNPs synthesis has been investigated in our previous study, and a summary of the findings is presented here.

Effect of pH

The optimal pH for AgNPs formation was determined by mixing 0.5 mL each of BR and MS extracts with 5 mL of 0.001 M AgNO₃ solution adjusted to different pH values (2, 4, 6, 8, and 10) using 0.1 M NaOH and HCl. As shown in Figure 1(a), no characteristic peak between 350 and 700 nm was observed at pH 2 and 4 for either extract mixture. However, a distinct peak emerged upon increasing the pH from 6 to 10, indicating the SPR of AgNPs.

The pH of the reaction mixture significantly affects the reduction process and the stability of the synthesized AgNPs. Alkaline conditions (higher pH) generally favor the formation of smaller AgNPs due to the enhanced electrostatic repulsion between the nanoparticles [27]. Increased alkalinity (pH) facilitates the hydrolysis of polyphenolic and flavonoid compounds present in both BR and MS extracts, rendering them more potent reducing agents for Ag⁺ ion reduction [28].

Effect of Extract Volume

To optimize the extract volume for AgNPs synthesis, 5 mL of 0.001 M AgNO₃ solution was prepared, followed by the addition of varying volumes of BR and MS extracts at the optimal pH and room temperature. As shown in Figure 1(b), the UV-Vis spectra revealed a red shift in the absorption peaks for both AgNPs.BR and AgNPs.MS with increasing extract volume (from 366 nm and 448 nm to 376 nm and 478 nm, respectively). This red shift suggests the formation of larger nanoparticles at higher extract concentrations. This phenomenon can be attributed to the presence of excess biomolecules interacting with the newly formed AgNPs at high extract concentrations, promoting further nucleation and

growth [27]. Conversely, the increasing intensity of the absorption peaks with increasing extract volume indicates a higher concentration of AgNPs in the reaction mixture [16].

Effect of Salt Concentration

The effect of AgNO₃ concentration on AgNPs formation is depicted in Figure 1(c). Notably, AgNPs.BR and AgNPs.MS were successfully synthesized at all precursor concentrations employed. Interestingly, the observed peaks broadened and shifted towards lower wavelengths with increasing AgNO₃ concentration. This trend suggests the continuous synthesis of AgNPs.BR and AgNPs.MS without significant agglomeration at higher silver ion concentrations. The increased availability of Ag⁺ ions in solution likely leads to the formation of more nanoparticles, influencing both their size and distribution [29]. The concentration of AgNO₃ solution significantly impacts the size and morphology of the biosynthesized AgNPs. Higher AgNO₃ concentrations generally lead to the formation of larger AgNPs due to the increased availability of silver ions for reduction.

Effect of reaction temperature

The influence of reaction temperature on the biosynthesis of AgNPs was investigated under optimized conditions. As depicted in Figure 1(d), the UV-Vis spectra show an increase in the biosynthesis of AgNPs for both BR and MS extracts with increasing temperature. The reaction temperature also influences the size and morphology of the AgNPs. Higher temperatures typically lead to the formation of larger AgNPs due to the increased reaction rate and aggregation of nanoparticles [30].

Effect of reaction time

In addition to the previously optimized conditions, the influence of reaction time on the biosynthesis of AgNPs was explored under various conditions (Figure 1(e)). It was observed that, with the AgNPs.MS, extending the reaction time from 10 to 120 minutes led to an increase in peak intensity, indicating

an increased yield of nanoparticles. Additionally, the peak sharpened, suggesting a more uniform size distribution [31].

However, the opposite trend was observed with the AgNPs.BR. While the formation of AgNPs.BR commenced promptly within 15 minutes, the optimal reaction time for obtaining a high yield and potentially more uniform particles was determined to be 60 minutes.

Mechanism of bioreduction and stabilization

The plant extracts of BR and MS are rich in various phytochemicals, particularly flavonoids and polyphenolic compounds, which play vital roles in both reducing and stabilizing the particles. The process commences with the addition of the extract to the AgNO₃ solution, wherein the phytochemicals donate electrons to Ag⁺ ions, which are then reduced to Ag⁰ atoms, leading to the formation of AgNPs [32]. The biomolecules then effectively cap the newly formed particles, preventing aggregation and stabilizing their structure.

In conclusion, optimal conditions for AgNPs.MS and AgNPs.BR production were identified, and the mechanism of bioreduction and stabilization was elucidated. It was found that AgNPs.MS formation is optimal at pH 8, an extract volume of 8 mL, and a reaction time of 120 minutes at 80°C, while AgNPs.BR formation is optimized at pH 10, an extract volume of 2 mL, and a reaction time of 60 minutes at room temperature.

Characterization of AgNPs.BR and AgNPs.MS

In order to study the properties of biosynthesized AgNPs using BR and MS extracts, various characterization techniques such as UV-Vis absorption spectra, FT-IR spectroscopy, XRD patterns, SEM and EMP were employed.

UV-Visible Spectroscopy

Figure 2 presents the UV-Vis absorption spectra of the colloidal AgNPs.BR and AgNPs.MS. The color change of the plant extracts from ruby red (BR) and pale pink (MS) to brown upon the addition of AgNO₃ indicates the formation of AgNPs.BR and AgNPs.MS, respectively. This phenomenon can be attributed to the excitation of SPR in the conducting electrons of the AgNPs. The biosynthesized AgNPs.BR and AgNPs.MS display maximum absorbance at 439 nm and 434 nm, respectively, which is consistent with the literature on silver nanoparticles [16, 33, 34].

Fourier-Transform Infrared (FT-IR) Spectroscopy

Figure 3 displays the FT-IR spectra of biosynthesized AgNPs.BR and AgNPs.MS under optimal conditions. A broad peak around 3400 cm⁻¹ is attributed to the O-H stretching vibration of polysaccharides present in the plant extracts. The peak observed at 2920-2950 cm⁻¹ corresponds to the C-H stretching vibration in alkanes or secondary amines [27]. The sharp peak around 1630 cm⁻¹ can be assigned to the stretching vibrations of C=C (alkene groups) and N-H (amide groups) [28]. Additionally, the presence of a band at 1380 cm⁻¹ suggests the presence of amide I bonds in proteins [33]. Peaks at 1050 cm⁻¹ and 605 cm⁻¹ can be attributed to C-O-C glycosidic linkages and out-of-plane C-H bending vibrations, respectively [35]. By comparing the FT-IR spectra of AgNPs and their respective extracts [25], the FT-IR spectrum of AgNPs.BR and AgNPs.MS showed the presence of polysaccharides and amid group as a reducing and stabilizing agent, respectively, which was in good agreement with other literature reports, it is evident that the primary functional groups present in the BR and MS extracts were responsible for the reduction of Ag⁺ ions to AgNPs.

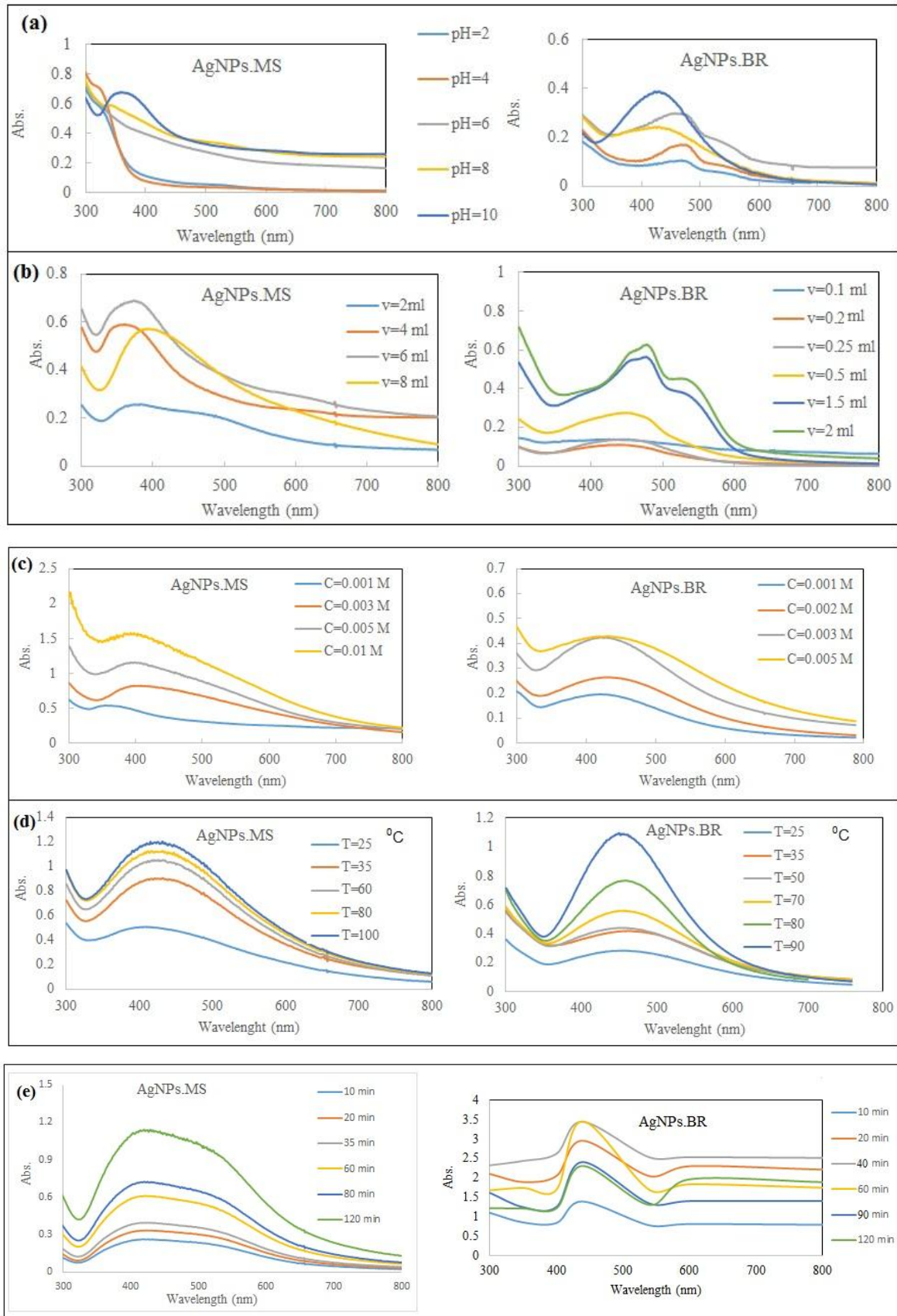


Figure 1. Effective parameters on synthesis of AgNPs using *Malva sylvestris* and *Beetroot* extract, a) Effect of pH; b) Effect of extract volume; c) Effect of salt concentration; (d) Effect of temperature and (e) Effect of time

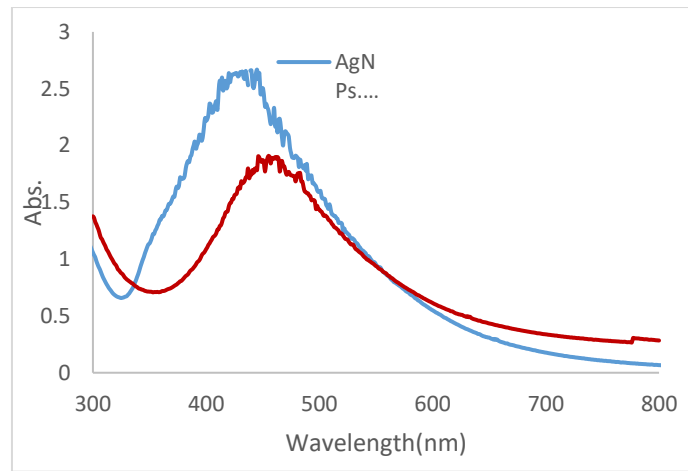


Figure 2. UV-Visible spectra of AgNPs using (a) *Beetroot* and (b) *Malva sylvestris* extract at optimum conditions

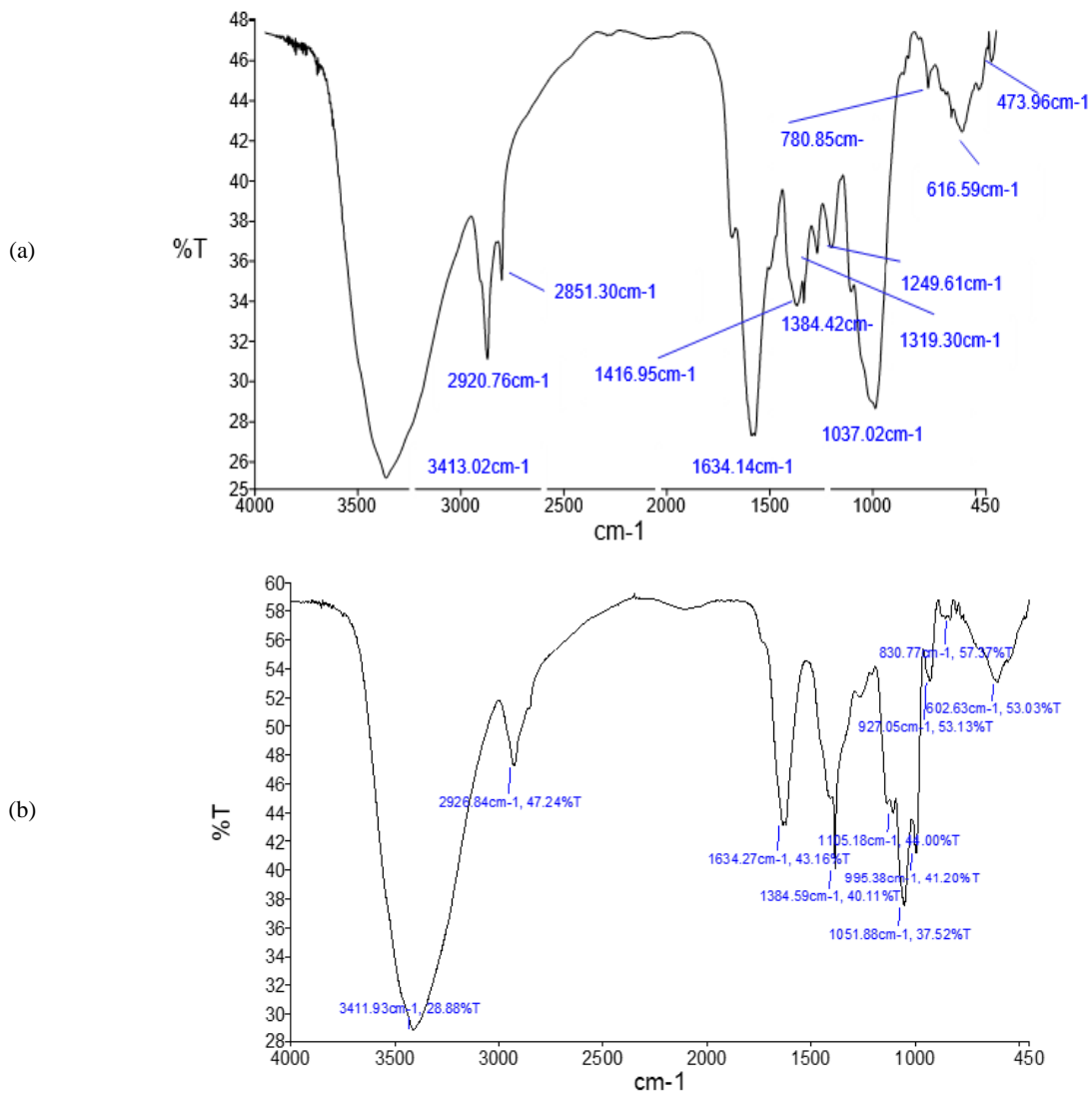


Figure 3. FT-IR spectra of AgNPs using (a) *Beetroot* and (b) *Malva sylvestris* extract

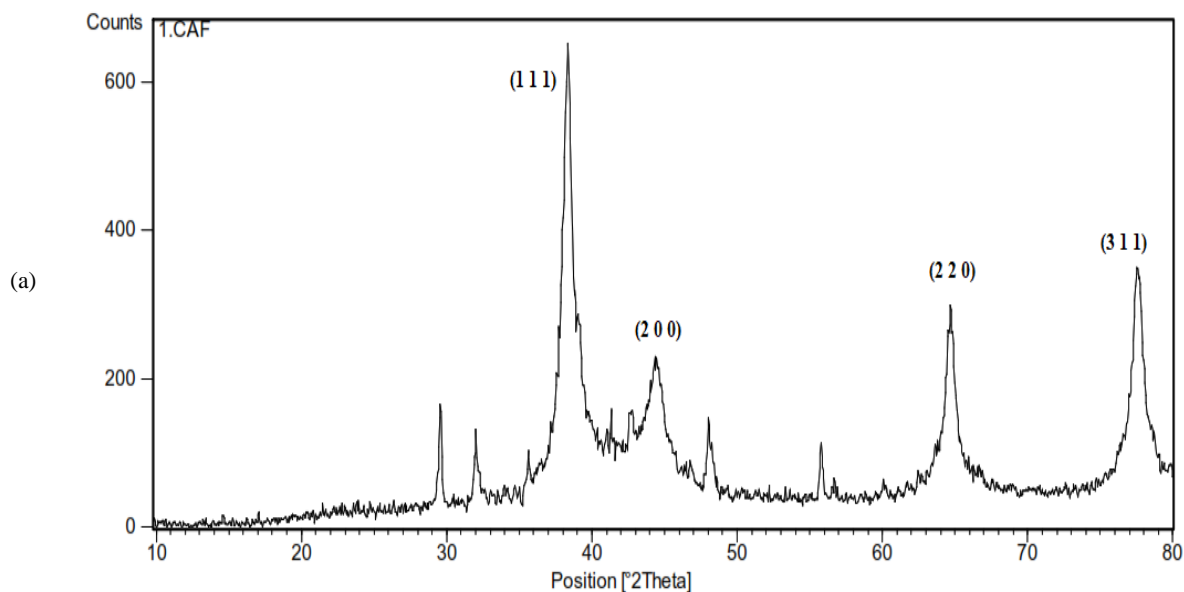
X-ray Diffraction (XRD) Analysis

The XRD patterns of dried AgNPs.BR and AgNPs.MS are shown in Figure 4. Both patterns display characteristic Ag peaks at 2θ values of 38° (111), 44.5° (200), 64.7° (220), and 77.7° (311), corresponding to the face-centered cubic crystal structure of silver nanoparticles [36]. These patterns were compared with the standard powder diffraction card of JCPDS silver No. 87-0717 for confirmation. Using Debye-Scherrer's equation, the average crystalline size of the AgNPs was calculated to be 18.5 nm for AgNPs.BR and 21.3 nm for AgNPs.MS.

SEM and TEM Analysis

SEM images (Figure 5) show the surface morphology of silver nanoparticles synthesized from BR and MS plant extracts. In image (a), the

nanoparticles are clustered and unevenly distributed on the surface. This clustered structure could be due to the aggregation of nanoparticles together, resulting in the formation of larger clumps. In image (b), the nanoparticles are more evenly distributed and dispersed on the surface. The structure of the nanoparticles in this image appears more regular and uniform compared to image (a). The more even and uniform distribution of nanoparticles in image (b) indicates better control over the synthesis process [37]. Further confirmation of the well-separated and non-agglomerated nature of the AgNPs is provided by the TEM images in Figure 6. The average size of the AgNPs.BR and AgNPs.MS in these images is approximately 20 nanometers, which corresponds well with the results obtained from the XRD patterns of these nanoparticles.



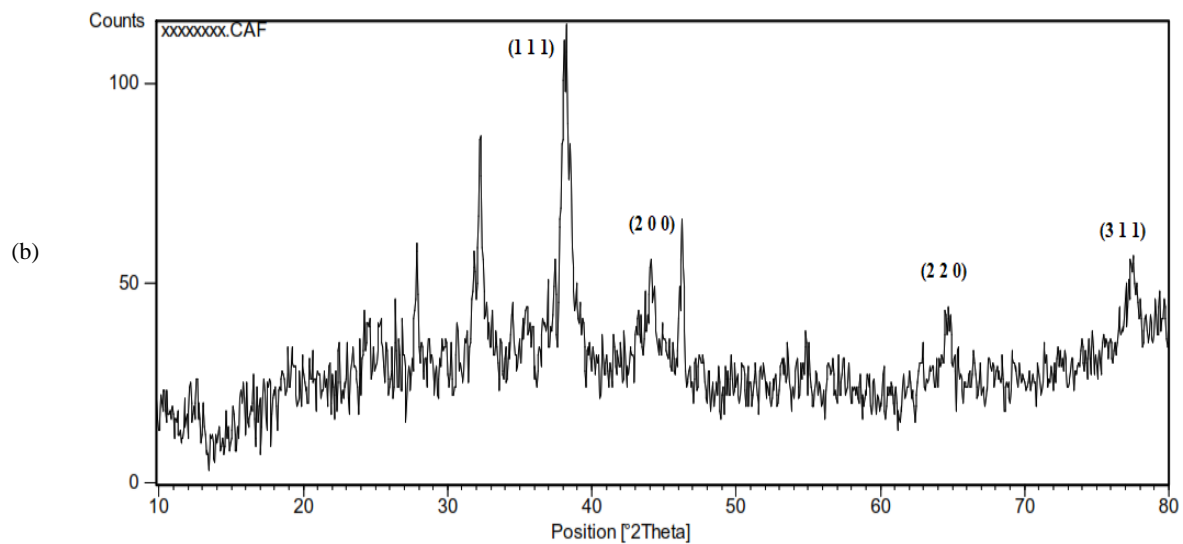


Figure 4. XRD pattern of AgNPs using (a) *Beetroot* and (b) *Malva sylvestris* extract

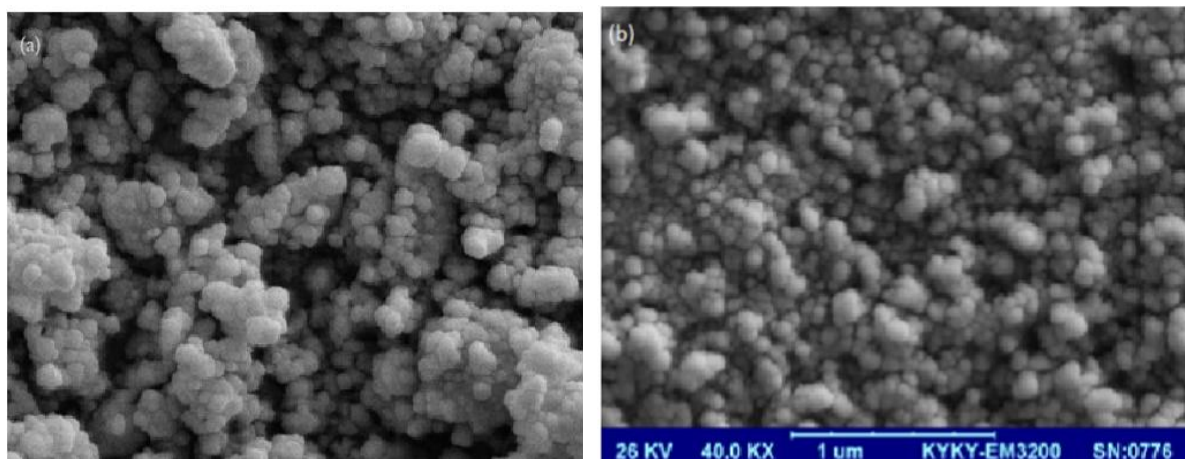


Figure 5. SEM images of AgNPs using (a) *Beetroot* and (b) *Malva sylvestris* extract

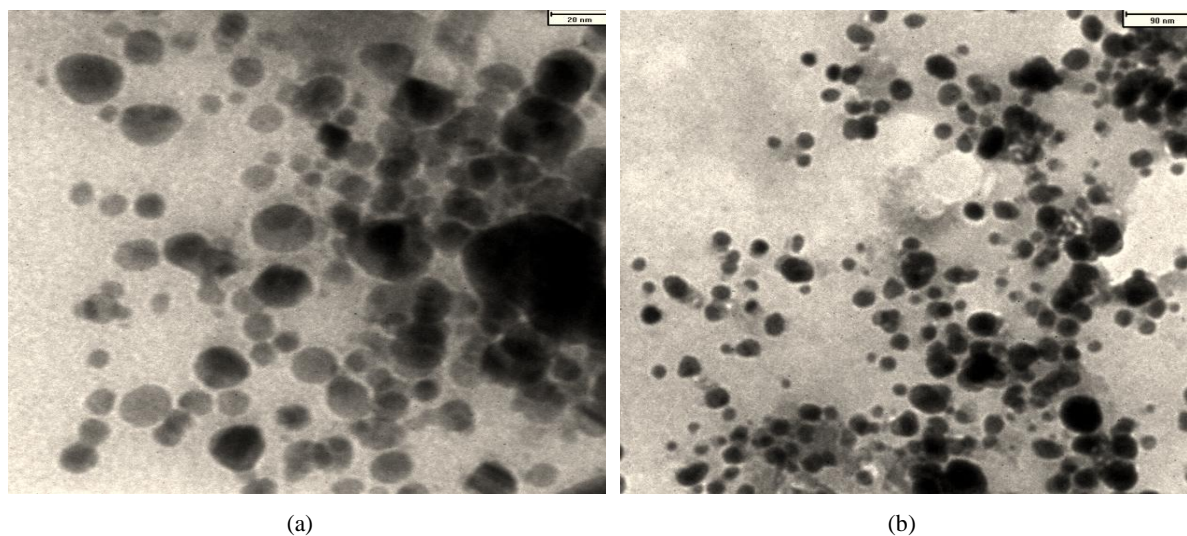


Figure 6. TEM images of AgNPs using (a) *Beetroot* and (b) *Malva sylvestris* extract

Catalytic activity of biosynthesized AgNPs for methylene blue degradation

AgNPs have gained significant attention due to their remarkable catalytic activity in various applications, including dye degradation [36]. This study investigates the catalytic efficiency of biosynthesized AgNPs.BR and AgNPs.MS extracts for the degradation of MB dye under ultrasonic irradiation.

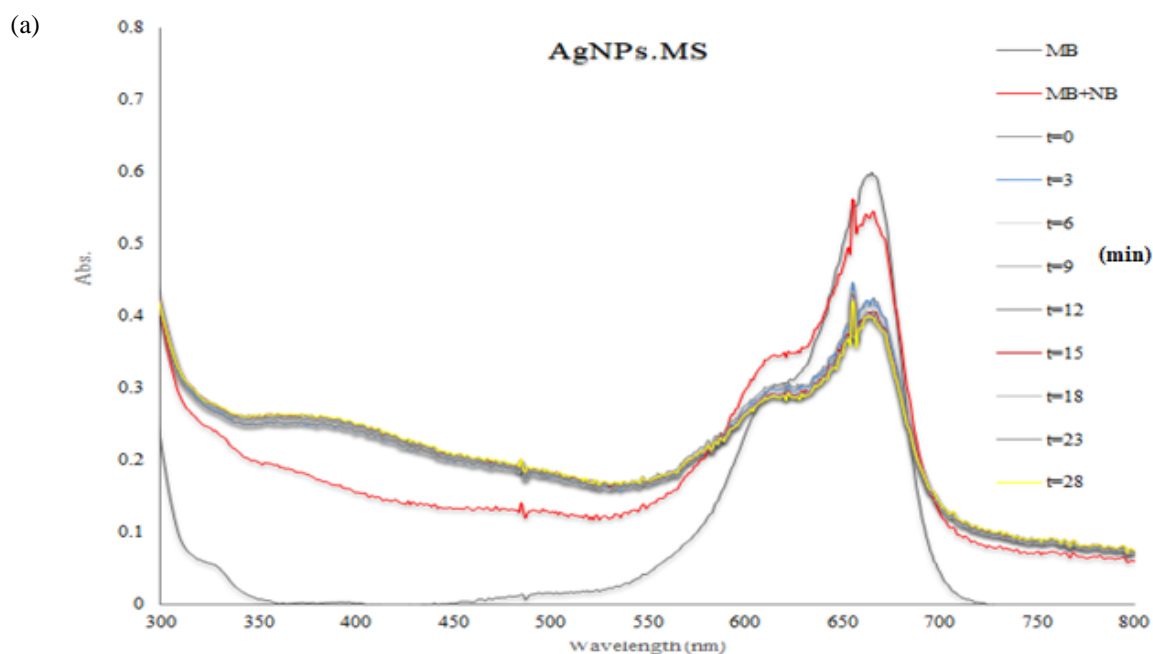
The catalytic activity of AgNPs.BR and AgNPs.MS was evaluated using MB dye and freshly prepared NaBH_4 as a reducing agent. The characteristic absorption peak of MB in its purified form was observed at 664 nm. The degradation mechanism can be explained by bonding dissociation energy theory, where the degradation reaction involves the breaking of chemical bonds in the MB molecule [34].

Figures 7(a) and 7(b) present the UV-Vis absorption spectra of MB solution treated with AgNPs.BR, AgNPs.MS, and a blank experiment with

NaBH_4 only. The significant decrease in the absorption peak intensity of MB at 664 nm in the presence of AgNPs.BR and AgNPs.MS confirms the effective reduction/degradation of the dye by these catalysts. This degradation likely occurs through a two-step process:

1. Adsorption: MB molecules are adsorbed onto the high surface area of the AgNPs due to weak van der Waals forces or electrostatic interactions.

2. Electron Transfer: Electrons from the reducing agent (BH_4^- ion) are transferred to the adsorbed MB molecules, facilitating their reduction to colorless degradation products [38]. The large surface area of the AgNPs acts as an electron relay, promoting this electron transfer process. The minimal change in absorbance observed in the blank experiment with NaBH_4 alone signifies the inability of NaBH_4 to effectively reduce MB without the catalyst.



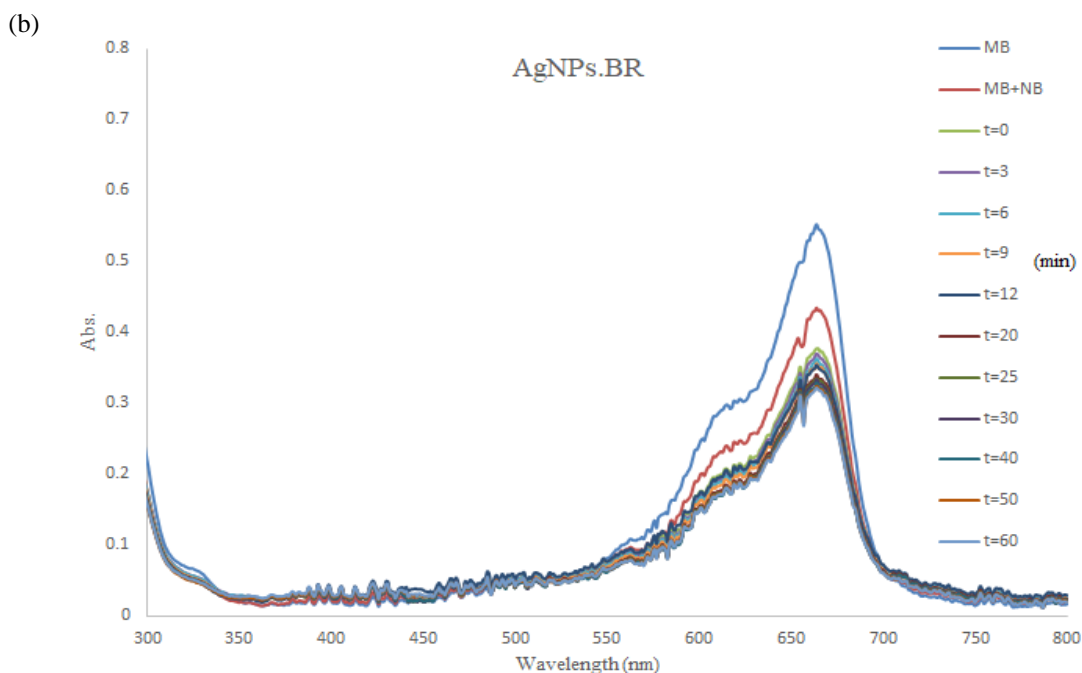


Figure 7. Catalytic activity of (a) AgNPs.BR and (b) AgNPs.MS in Methylene blue reduction in presence and absence of NaBH_4

Kinetic Analysis

To quantify the degradation rate of MB, the data will be further analyzed using various kinetic models, including pseudo-first-order, pseudo-second-order, intra-particle diffusion, and Elovich equations [39, 40]. The linear form of the pseudo-first-order equation (Eq. 1) will be used as an initial step for the kinetic analysis:

$$\log(q_e - q_t) = \log q_e - \frac{k_1 t}{2.303} \quad (1)$$

The linear form of the pseudo-second-order equation (Eq. 2) is expressed below:

$$\frac{t}{q_t} = \frac{1}{k_2 q_e^2} + \frac{1}{q_e} t \quad (2)$$

Where q_e and q_t (mg/g) represent the equilibrium concentration and the concentration of MB at time t , respectively. k_1 (min^{-1}) and k_2 ($\text{g}/(\text{mg}\cdot\text{min})$) are the rate constants for the pseudo-first-order and pseudo-second-order models, respectively.

In addition to the pseudo-first-order and pseudo-second-order models, the kinetic data were further analyzed using the intra-particle diffusion and Elovich models. The linear forms of these equations

are presented below:

Intra-particle diffusion equation (Eq. 3):

$$q_t = k_i t^{1/2} + I \quad (3)$$

Where, q_t (mg/g) is the amount of MB adsorbed at time t , k_i ($\text{mg}/(\text{g}\cdot\text{min}^{0.5})$) is the intra-particle diffusion rate constant, I (mg/g) is a constant related to the boundary layer thickness, t (min) is the reaction time.

Elovich equation (Eq. 4):

$$q_t = \beta \ln(\alpha\beta) + \beta \ln t \quad (4)$$

Where, α ($\text{mg}/(\text{g}\cdot\text{min})$) is the initial adsorption rate, β (mg/g) is the desorption coefficient and t (min) is the reaction time.

The analysis of kinetic data (Figures 8, 9 and Table 1) using various models revealed the following:

The pseudo-first-order model: Both AgNPs (AgNPs.BR and AgNPs.MS) have the same q_e (0.001 mg/g). This indicates that both AgNPs are capable of adsorbing a similar amount of MB. k_1 for AgNPs.MS (0.097 min^{-1}) is approximately 4 times higher than that of AgNPs.BR (0.024 min^{-1}). This suggests that the reaction rate is faster for AgNPs.MS. R^2 is high for

both AgNPs (0.9705 and 0.987), indicating that the pseudo-first-order model fits the data well for both AgNPs. However, R^2 for AgNPs.MS (0.987) is slightly higher than that of AgNPs.BR (0.9705), suggesting that the pseudo-first-order model fits slightly better for AgNPs.MS. Based on the data provided, it appears that the pseudo-first-order model fits the data well for both AgNPs.

The pseudo-second-order model: q_e for AgNPs.MS (0.004 mg/g) is slightly higher than that of AgNPs.BR (0.0037 mg/g). This indicates that AgNPs.MS is capable of adsorbing a slightly higher amount of MB. k_2 for AgNPs.MS (228.64 g/(mg.min)) is significantly (approximately 17%) higher than that of AgNPs.BR (195.45 g/(mg.min)). This suggests that the reaction rate for nanoparticles synthesized from AgNPs.MS is faster in the pseudo-second-order model. R^2 for both AgNPs is very high (0.998 and 0.999), indicating that the pseudo-second-order model fits the data well for both AgNPs. However, R^2 for AgNPs.MS (0.999) is slightly higher than that of AgNPs.BR (0.998), suggesting that the pseudo-second-order model fits slightly better for AgNPs.MS.

The intraparticle diffusion model: The intraparticle diffusion model is one of the models used to study the mechanisms of adsorption in the removal of pollutants from aqueous solutions. This model is particularly useful for understanding the adsorption processes within the adsorbent particles and can provide insights into the rate and mechanism of pollutant diffusion inside the adsorbent. The results indicated that both types of silver nanoparticles exhibited significant potential for MB dye removal. However, silver nanoparticles synthesized from MS

extract demonstrated a higher intraparticle diffusion rate constant $k_i = 0.0002$ (mg/(g.min^{0.5})) compared to those synthesized from BR extract $k_i = 0.0001$ (mg/(g.min^{0.5})). This suggests a more efficient diffusion process within the MS-based nanoparticles. Additionally, the higher boundary layer constant ($I = 0.0032$ mg/g) and the closer fit of the model ($R^2 = 0.979$) for MS-based nanoparticles further support their superior adsorption performance. The BR-based nanoparticles, while effective, showed a slightly lower diffusion rate and model fit ($R^2 = 0.976$).

The Elovich model: α for AgNPs.MS (102464600 mg/(g.min)) is significantly (approximately 10300 times) higher than that of AgNPs.BR (9936500 mg/(g.min)). This indicates that the initial adsorption rate for nanoparticles synthesized from MS extract is much faster in the Elovich model. α (mg/(g.min)) is also significantly (approximately 10 times) higher for AgNPs.MS (320.35 mg/(g.min)) than for AgNPs.BR (31.006 mg/(g.min)). This further confirms the higher initial adsorption rate for nanoparticles synthesized from MS extract. β is nearly the same for both AgNPs (0.0003 mg/g for AgNPs.BR and 0.0003 mg/g for AgNPs.MS). This parameter is related to the surface saturation capacity for adsorption, and the similarity in values for the two AgNPs suggests that the surface saturation capacity for adsorption of silver nanoparticles is similar in both cases. R^2 is high for both AgNPs (0.969 and 0.9784), indicating that the Elovich model fits the data well for both AgNPs. However, R^2 for AgNPs.MS (0.9784) is slightly higher than that of AgNPs.BR (0.969), suggesting that the Elovich model fits slightly better for AgNPs.MS.

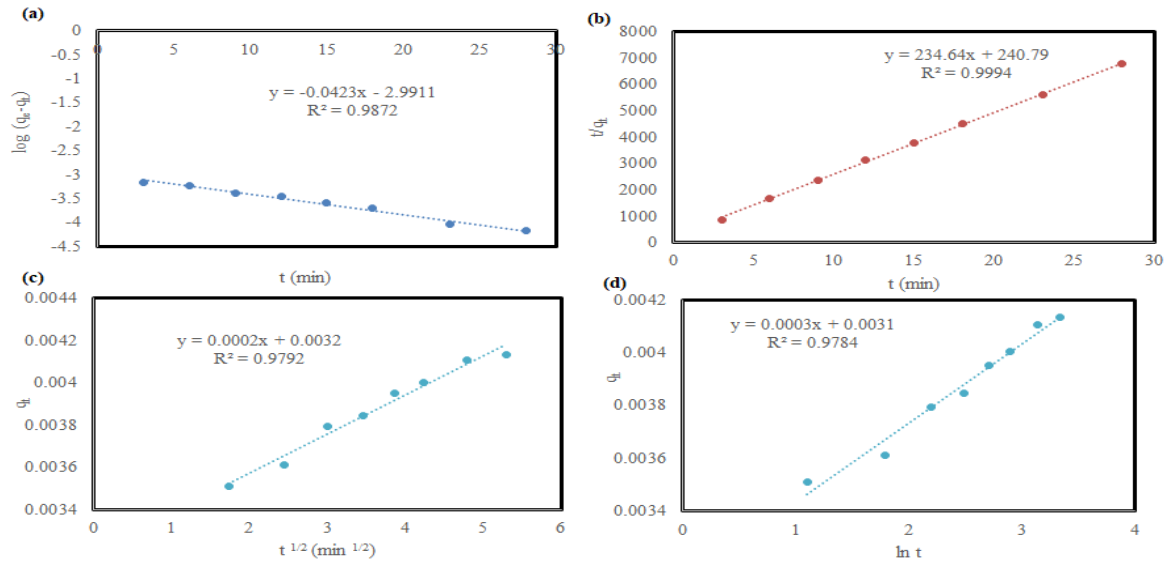


Figure 8. (a) pseudo first order; (b) pseudo second order, type 1; (c) pseudo second order, type 2; (d) pseudo second order, type 3 (e) pseudo second order, type 4; (f) intra particle diffusion and (g) Elovich equation of AgNPs.MS

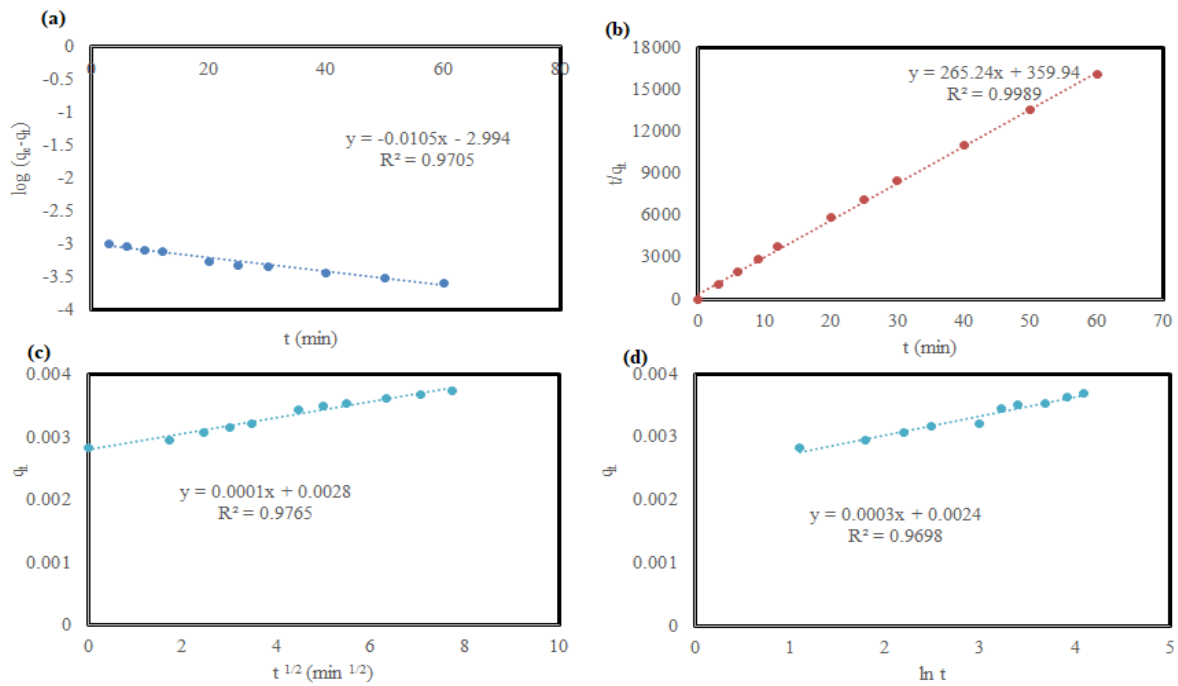


Figure 9. (a) pseudo first order; (b) pseudo second order (c) intra particle diffusion and (d) Elovich equation of AgNPs.BR

Table 1. The kinetics parameters for catalytic activity of methylene blue onto AgNPs-BR and AgNPs-MS

Model	Parameter	silver nanoparticles	
		<i>Beetroot</i> extract	<i>Malva sylvestris</i> extract
Pseudo-first-order	q_e (mg/g)	0.001	0.001
	k_1 (min^{-1})	0.024	0.097

	R ²	0.9705	0.987
Pseudo-second-order	q _e (mg/g)	0.0037	0.004
	k ₂ (g/(mg.min))	195.45	228.64
	R ²	0.998	0.999
Intra particle diffusion	k _i (mg/(g.min ^{0.5}))	0.0001	0.0002
	I (mg/g)	0.0028	0.0032
	R ²	0.976	0.979
Elovich	α (mg/(g.min))	9936500	102464600
	β (mg/g)	0.0003	0.0003
	R ²	0.969	0.9784

CONCLUSION

This study successfully demonstrated the biosynthesis of AgNPs using aqueous extracts of MS and BR. The phenolic and flavonoid compounds in these extracts acted as efficient reducing and stabilizing agents. A comprehensive examination of various synthesis parameters, including pH, extract volume, salt concentration, temperature, and time, revealed their significant influence on the crystal size of AgNPs.

The biosynthesized nanoparticles were characterized using several techniques, including UV-Vis spectrophotometry, FT-IR, XRD, SEM, and TEM. Both types of AgNPs exhibited a face-centered cubic (FCC) crystal structure, with maximum absorbance peaks at 439 nm for AgNPs.BR and 434 nm for AgNPs.MS. Catalytic activity in the reduction of MB was confirmed through surface plasmon resonance spectroscopy. Kinetic data were analyzed using pseudo-first-order, pseudo-second-order, intraparticle diffusion, and Elovich models. The accelerated reduction of MB in the presence of 0.008 g AgNPs.BR and 0.005 g AgNPs.MS, with rate constants of 0.024 min⁻¹ and 0.097 min⁻¹ respectively, highlighted the substantial catalytic potential of these nanoparticles.

The findings of this research indicate that

plant extracts can be effectively utilized for the biosynthesis of silver nanoparticles, offering a simple, environmentally friendly method with significant catalytic applications.

ACKNOWLEDGEMENT

The authors would like to thank the Islamic Azad University, Arak Branch, for providing the laboratory equipment necessary for conducting this research.

REFERENCES

1. Ali I, Gupta VK. Advances in water treatment by adsorption technology. *Nat. Protoc.* 2006;1(8):2661-7. <https://doi.org/10.1038/nprot.2006.370>.
2. Forgacs E, Cserháti T, Oros G. Removal of synthetic dyes from wastewaters: a review. *Environ. Int.* 2004;30(7):953-71. <https://doi.org/10.1016/j.envint.2004.02.001>.
3. Rai M, Yadav A, Gade A. Silver nanoparticles as a new generation of antimicrobials. *Biotechnol. Adv.* 2009;27(1):76-83. <https://doi.org/10.1016/j.biotechadv.2008.09.002>.
4. Ahmed S, Ahmad M, Swami BL, Ikram S. A review on plants extract mediated synthesis of silver nanoparticles for antimicrobial applications:

- a green expertise. J. Adv. Res. 2016;7(1):17-28. <https://doi.org/10.1016/j.jare.2015.02.007>.
5. Prabhu S, Poulouse EK. Silver nanoparticles: mechanism of antimicrobial action, synthesis, medical applications, and toxicity effects. Int. Nano Lett. 2012;2(1):32. <https://doi.org/10.1186/2228-5326-2-32>.
 6. Iravani S, Korbekandi H, Mirmohammadi SV, Zolfaghari B. Synthesis of silver nanoparticles: chemical, physical and biological methods. Res. Pharm. Sci. 2014;9(6):385-406.
 7. Ghaedi M, Yousefinejad M, Safarpour M, Zare-Khafri H, Purkait MK. *Rosmarinus officinalis* leaf extract mediated green synthesis of silver nanoparticles and investigation of its antimicrobial properties. J Ind Eng Chem. 2015;31:167-172. <https://doi.org/10.1016/j.jiec.2015.06.020>
 8. Luna C, Chávez VH, Barriga-Castro ED, Núñez NO, Mendoza-Reséndez R. Biosynthesis of silver fine particles and particles decorated with nanoparticles using the extract of *Illicium verum* (star anise) seeds. Spectrochim. Acta A Mol. Biomol. Spectrosc. 2015;141:43-50. <http://dx.doi.org/10.1016/j.saa.2014.12.076>.
 9. Ashokkumar S, Ravi S, Velmurugan S. Green synthesis of silver nanoparticles from *Gloriosa superba L.* leaf extract and their catalytic activity. Spectrochim. Acta A Mol. Biomol. Spectrosc. 2013;115:388-392. <http://dx.doi.org/10.1016/j.saa.2013.06.050>.
 10. Saravanakumar A, Ganesh M, Jayaprakash J, Jang HT. Biosynthesis of silver nanoparticles using *Cassia tora* leaf extract and its antioxidant and antibacterial activities. J. Ind. Eng. Chem. 2015;28:277-281. <http://dx.doi.org/10.1016/j.jiec.2015.03.003>.
 11. Allafchian AR, Mirahmadi-Zare SZ, Jalali SAH, Hashemi SS, Vahabi MR. Green synthesis of silver nanoparticles using *phlomis* leaf extract and investigation of their antibacterial activity. J Nanostruct Chem. 2016;6:129-35. <https://doi.org/10.1007/s40097-016-0187-0>.
 12. Sedaghat S, Agbolag AE, Bagheriyan S. Biosynthesis of silver nanoparticles using *pennyroyal* water extract as a green route. J Nanostruct Chem. 2016;6:25-7. <https://doi.org/10.1007/s40097-015-0176-8>.
 13. Nasiri J, Rahimi M, Hamezadeh Z, Motamedi E, Naghavi MR. Fulfillment of green chemistry for synthesis of silver nanoparticles using root and leaf extracts of *Ferula persica*: Solid-state route vs. solution-phase method. J. Clean. Prod. 2018;192:514-530. <https://doi.org/10.1016/j.jclepro.2018.04.218>.
 14. Ajitha B, Reddy YAK, Reddy PS. Green synthesis and characterization of silver nanoparticles using *Lantana camara* leaf extract. Mater. Sci. Eng. C. 2015;49:373-381. <https://doi.org/10.1016/j.msec.2015.01.035>.
 15. Mo YY, Tang YK, Wang SY, Lin JM, Zhang HB, Luo DY. Green synthesis of silver nanoparticles using *eucalyptus* leaf extract. Mater. Lett. 2015;144:165-177. <https://doi.org/10.1016/j.matlet.2015.01.004>.
 16. Zayed MF, Eisa WH, Shabaka AA. *Malva parviflora* extract assisted green synthesis of silver nanoparticles. Spectrochim. Acta A Mol. Biomol. Spectrosc. 2012;98:423-428. <https://doi.org/10.1016/j.saa.2012.08.072>.
 17. Pattanayak S, Mollick M, Maity D, Chakraborty S, Dash SK, Chattopadhyay S, Roy S, Chattopadhyay D, Chakraborty M. *Butea monosperma* bark extract mediated green synthesis of silver nanoparticles: Characterization and biomedical applications. J. Saudi Chem. Soc. 2017;21(6):673-84. <https://doi.org/10.1016/j.jscs.2015.11.004>.
 18. Ramar M, Manikandan B, Raman T, Arunagirinathan K, Prabhu NM, Basu MJ, Perumal M, Palanisamy S, Munusamy A.

- Biosynthesis of silver nanoparticles using ethanolic petals extract of *Rosa indica* and characterization of its antibacterial, anticancer and anti-inflammatory activities. *Spectrochim. Acta A Mol. Biomol. Spectrosc.* 2015;138:120-9. <https://doi.org/10.1016/j.saa.2014.10.043>.
19. Moond M, Singh S, Sangwan S, Devi P, Beniwal A, Rani J, Kumari A, Rani S. Biosynthesis of Silver Nanoparticles Utilizing Leaf Extract of *Trigonella foenum-graecum L.* for Catalytic Dyes Degradation and Colorimetric Sensing of Fe³⁺/Hg²⁺. *Molecules.* 2023;28(3):951. <https://doi.org/10.3390/molecules28030951>.
20. Samari F, Salehipoor H, Eftekhari E, Yousefinejad S. Low-temperature biosynthesis of silver nanoparticles using *mango* leaf extract: catalytic effect, antioxidant properties, anticancer activity and application for colorimetric sensing. *New J. Chem.* 2018;42:15905-16. <https://doi.org/10.1039/C8NJ03156H>.
21. Sharmin S, Islam M, Kanti Saha B, Ahmed F, Maitra B, Rasel M, Quaisar N, Rabbi M. Evaluation of antibacterial activity, in-vitro cytotoxicity and catalytic activity of biologically synthesized silver nanoparticles using leaf extracts of *Leea macrophylla*. *Heliyon.* 2023;9(1):e20810. <https://doi.org/10.1016/j.heliyon.2023.e20810>.
22. Sooraj MP, Nair AS, Vineetha D. Sunlight-mediated green synthesis of silver nanoparticles using *Sida retusa* leaf extract and assessment of its antimicrobial and catalytic activities. *Chem. Pap.* 2021;75(1):351-63. <https://doi.org/10.1007/s11696-020-01304-0>.
23. Raikos V, McDonagh A, Ranawana V, Duthie G. Processed beetroot (*Beta vulgaris L.*) as a natural antioxidant in mayonnaise: Effects on physical stability, texture and sensory attributes. *Food Sci. Hum. Wellness.* 2016;5(4):191-8. <https://doi.org/10.1016/j.fshw.2016.10.002>.
24. Carrillo C, Wilches-Perez D, Hallmann E, Kazmierczak R, Rembiałkowska E. Organic versus conventional beetroot. Bioactive compounds and antioxidant properties. *LWT.* 2019;116:108552. <https://doi.org/10.1016/j.lwt.2019.108552>.
25. Mehdizadeh S, Ghasemi N, Ramezani M. The synthesis of silver nanoparticles using Beetroot extract and its antibacterial and catalytic activity. *Eurasian Chem. Commun.* 2019;1(6):545-58. <https://doi.org/10.22034/ECC.2019.1960614.1004>.
26. Mehdizadeh S, Ghasemi N, Ramezani M, Mahanpoor K. Biosynthesis of Silver Nanoparticles Using *Malva sylvestris* Flower Extract and Its Antibacterial and Catalytic Activity. *Chem. Methodol.* 2021;5(4): 356-366. <https://doi.org/10.22034/chemm.2021.132490>.
27. Mosaviniya M, Kikhavani T, Tanzifi M, Tavakkoli-Yaraki M, Tajbakhsh P, Lajevardi A. Facile green synthesis of silver nanoparticles using *Crocus haussknechtii* *Bois bulb* extract: Catalytic activity and antibacterial properties. *Colloid Interface Sci. Commun.* 2019;33:100211. <https://doi.org/10.1016/j.colcom.2019.100211>.
28. Nouri A, Yarak MT, Lajevardi A, Rezaei Z, Ghorbanpour M, Tanzifi M. Ultrasonic-assisted green synthesis of silver nanoparticles using *Mentha aquatica* leaf extract for enhanced antibacterial properties and catalytic activity. *Colloid Interface Sci. Commun.* 2020;35:100252. <https://doi.org/10.1016/j.colcom.2020.100252>.
29. Chen J, Wang J, Zhang X, Jin Y. Microwave-assisted green synthesis of silver nanoparticles by carboxymethyl cellulose sodium and silver nitrate. *Mater. Chem. Phys.* 2008;108:421-4. <https://doi.org/10.1016/j.matchemphys.2007.10.019>.



30. Kazemi S, Hosseingholian A, Gohari SD, Feirahi F, Moammeri F, Mesbahian G, Moghaddam ZS, Ren Q. Recent advances in green synthesized nanoparticles: From production to application. *Mater. Today Sustain.* 2023;24:100500. <https://doi.org/10.1016/j.mtsust.2023.100500>.
31. Zeng J, Xiong X, Hu F, Li J, Li P. Dialdehyde Cellulose Solution as Reducing Agent: Preparation of Uniform Silver Nanoparticles and In Situ Synthesis of Antibacterial Composite Films with High Barrier Properties. *Molecules.* 2023;28(7):2956. <https://doi.org/10.3390/molecules28072956>.
32. Ghasemi S, Dabirian S, Kariminejad F, et al. Process optimization for green synthesis of silver nanoparticles using *Rubus discolor* leaves extract and its biological activities against multi-drug resistant bacteria and cancer cells. *Sci. Rep.* 2024;14:4130. <https://doi.org/10.1038/s41598-024-54702-9>.
33. Hamed S, Shojaosadati SA. Rapid and green synthesis of silver nanoparticles using *Diospyros lotus* extract: Evaluation of their biological and catalytic activities. *Polyhedron.* 2019;171:172-80. <https://doi.org/10.1016/j.poly.2019.07.010>.
34. Aadil KR, Pandey N, Mussatto SI, Jha H. Green synthesis of silver nanoparticles using *acacia lignin*, their cytotoxicity, catalytic, metal ion sensing capability and antibacterial activity. *J. Environ. Chem. Eng.* 2019;7:103296. <https://doi.org/10.1016/j.jece.2019.103296>.
35. Ghaedi M, Yousefinejad M, Safarpour M, Zare-Khafri H, Purkait MK. *Rosmarinus officinalis* leaf extract mediated green synthesis of silver nanoparticles and investigation of its antimicrobial properties. *J. Ind. Eng. Chem.* 2015;31:167-72. <http://dx.doi.org/10.1016/j.jiec.2015.06.020>.
36. Kahraman HT. Synthesis of silver nanoparticles using *Alchemilla vulgaris* and *Helichrysum arenarium* for methylene blue and 4-nitrophenol degradation and antibacterial applications. *Biomass Convers. Bioref.* 2024;14:13479-90. <https://doi.org/10.1007/s13399-024-05314-w>.
37. Wang X, Fang X, Liu X, Lyu Y, Ma L, Fu J. Spike nanoparticles: From design to biomedical applications. *Next Mater.* 2024;2:100080. <https://doi.org/10.1016/j.nxmate.2023.100080>.
38. Ganguly S, Mondal S, Das P, Bhawal P, Das TK, Bose M, Choudhary S, Gangopadhyay S, Das AK, Das NC. Natural saponin stabilized nano-catalyst as efficient dye-degradation catalyst. *Nano-Struct. Nano-Obj.* 2018;16:86-95. <https://doi.org/10.1016/j.nanoso.2018.05.002>.
39. Ghasemi M, Javadian H, Ghasemi N, Agarwal S, Gupta VK. Microporous nanocrystalline NaA zeolite prepared by microwave assisted hydrothermal method and determination of kinetic, isotherm and thermodynamic parameters of the batch sorption of Ni (II). *J. Mol. Liq.* 2016;215:161-9. <http://dx.doi.org/10.1016/j.molliq.2015.12.038>.
40. Ghasemi M, Naushad M, Ghasemi N, Khosravi-Fard Y. Adsorption of Pb(II) from aqueous solution using new adsorbents prepared from agricultural waste: Adsorption isotherm and kinetic studies. *J. Ind. Eng. Chem.* 2014;20:2193-9. <http://dx.doi.org/10.1016/j.jiec.2013.09.050>.